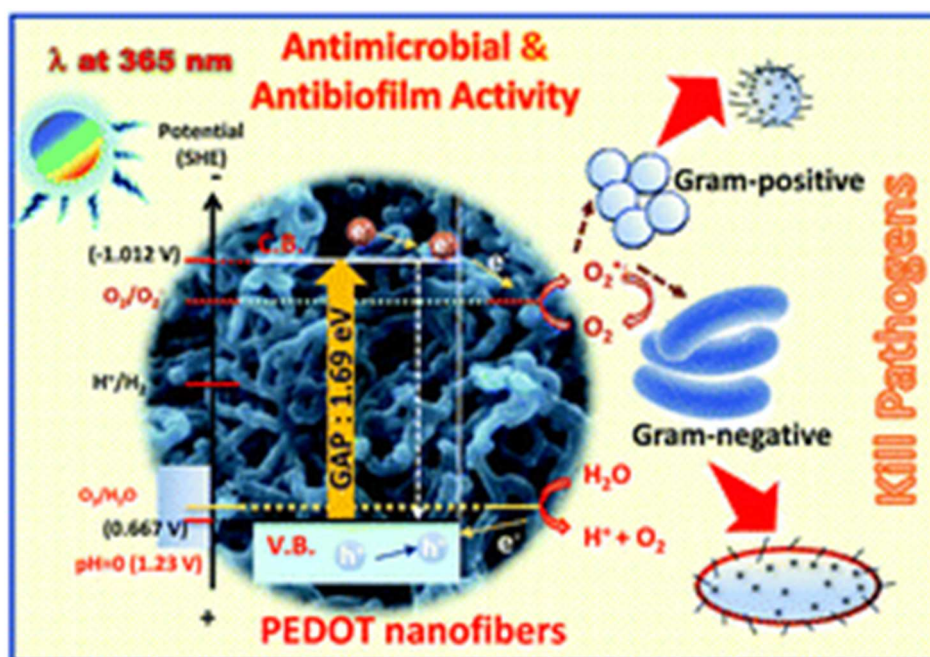


Conjugated polymer nanostructures displaying high photoactivated antimicrobial and antibiofilm functionalities

Please, cite as follows:

Srabanti Ghosh, Marta Elena Gonzalez-Mosquera, Georgiana Amariei, Roberto Rosal. Conjugated polymer nanostructures displaying high photoactivated antimicrobial and antibiofilm functionalities, *Journal of Materials Chemistry B*, 2021, 9, 4390-4399, <https://doi.org/10.1039/D1TB00469G>



<https://pubs.rsc.org/en/content/articlelanding/2021/tb/d1tb00469g>

Conjugated polymer nanostructures displaying high photoactivated antimicrobial and antibiofilm functionalities

Srabanti Ghosh^{1,†,*}, Marta Elena Gonzalez-Mosquera^{1,*}, Georgiana Amariei², Roberto Rosal²

¹ Department of Organic and Inorganic Chemistry, Institute of Chemical Research “Andrés M. del Río” (IQAR), Universidad de Alcalá, 28805 Alcalá de Henares, Madrid, Spain.

² Department of Chemical Engineering, Universidad de Alcalá, 28805 Alcalá de Henares, Madrid, Spain.

[†] Present address: Energy Materials & Devices Division, CSIR-Central Glass and Ceramic Research Institute, Kolkata-700032, India.

* Corresponding Authors martaeg.mosquera@uah.es, srabanti@cgcri.res.in

Abstract

This work reports the use of conjugated polymer nanostructures (CPNs) as photoactivated antimicrobial compounds against gram-positive and gram-negative microorganisms. Two representative CPNs of polythiophene (PEDOT) and polyaniline (PANI) were prepared as nanofibres with average diameter of 40 nm and length in the micrometer range. Both CPNs exhibited strong antimicrobial activity under UVA irradiation with the same fluence rate as the UVA component of the solar spectrum. The effect was tested using the gram-positive bacteria *Staphylococcus aureus* and the gram-negative bacteria *Escherichia coli*. The reduction of colony forming units (CFU) reached > 6-log for PEDOT concentrations as low as 33 ng mL⁻¹. For PEDOT nanofibers, a complete inhibition of *S. aureus* and *E. coli* growth was reached at 883 ng mL⁻¹ and 333 ng mL⁻¹ respectively. The photoactivated effect of PANI nanofibres to *S. aureus* and *E. coli* was also high, with CFU reduction of about 7-log and 4-log respectively for exposure concentration of 33 ng mL⁻¹. The antimicrobial activity was only high under light irradiation and was almost negligible for bulk PEDOT and PANI. The effect of polymeric nanofibers could be attributed to the photoinduced generation of reactive oxygen species, which may induce cell membrane damage, eventually leading to bacterial impairment and inhibition of their biofilm forming capacity. CPN PEDOT and PANI coatings were able to keep surfaces free of bacterial attachment and growth even after 20 h of previous contact with exponentially growing cultures in dark. PEDOT and PANI CPNs demonstrated good cytocompatibility with human fibroblasts and absence of haemolytic activity. The materials demonstrated advantages in terms of broad antibacterial spectrum, biofilms inhibition, and absence of acute toxicity for biomedical applications.

1. Introduction

Conjugated polymers hold a great promise to meet the increasing demand for biosensing, imaging and therapy, advanced energy storage, and pollutant removal to mitigate environmental problems, due to their superior optical properties, low cost, and biocompatibility.¹⁻³ Recently, conjugated polymer nanostructures (CPNs) have been identified as a new generation photoactive materials that display high electrical conductivity and electrochemical activity, which make them ideal for energy conversion and storage.⁴⁻⁵ A considerable success has also been achieved using CPNs as active materials in the field of photocatalysis such as visible light induced organic pollutants removal and water splitting for hydrogen production.⁶⁻⁹ As well, functionalized conjugated polymer nanoparticles have been proposed for photo-triggered delivery of biological agents.¹⁰ Furthermore, conductive polymers have been used to prepare bioelectronic devices taking advantage of their excellent mechanical properties compared to inorganic materials.¹¹

However, an important problem of polymers in biological media is their easy fouling due to the nonspecific adsorption of proteins and other organic substances. Two main strategies had been followed to produce antifouling conducting polymers, namely the introduction of antifouling moieties with the monomers or the post-functionalization by grafting hydrophilic units onto the polymeric surface.¹² Protein adsorption has been avoided by means of covalent bonding of non-ionic polymers like poly(ethylene glycol), or zwitterionic polymers that showed high fouling resistance due to electrostatic interactions.¹³

As well, it has been shown that conducting polymers, such as colloidal dispersions of polyaniline (PANI) showed certain antimicrobial effect which attributed to electrostatic interaction between the polymer and bacterial envelopes.¹⁴ However, the effect is weak and the reported minimum inhibitory concentrations against *Escherichia coli* (*E. coli*) and *Staphylococcus aureus* (*S. aureus*) were as high as 3500 µg mL⁻¹ and 8500 µg mL⁻¹.¹⁵ The antimicrobial properties of conductive polyanilines had been successfully

enhanced by co-polymerizing aniline with poly(aniline-co-3-aminobenzoic acid).¹⁶ Another modification of conductive polymers that enhanced their antimicrobial properties is the introduction of metals. Accordingly, copper nanoparticles dispersed in PANI showed antimicrobial effect against several strains due to the release of copper ions.¹⁷ In another study, PANI/Au-Pd bimetallic nanocomposites exhibited significant antibacterial activity, with minimum inhibitory concentration of 25 $\mu\text{g mL}^{-1}$, which strongly depended on metal particle size and was probably due to the interaction of metal nanoparticles with bacterial walls.¹⁸ Nanocomposites containing poly(3,4-ethylenedioxythiophene) have also showed antimicrobial behavior when enhanced using approaches such as the diffusion of fluoride from fluorohydroxyapatite nanoparticles or the inclusion of magnetic iron oxide nanoparticles to promote a photothermal effect.¹⁹⁻²⁰

Biofouling refers to the undesired growth of biofilms on surfaces exposed to microbial growth. Biofilms are an evolutive strategy for microorganisms to colonize surfaces with the aid of a self-produced matrix of extracellular polymeric materials and a complex sessile structure.²¹ Once attached to a surface, microbial biofilms are very difficult to eradicate and, therefore, significant efforts have been made to fabricate materials and coatings that prevent biofilm formation by inhibiting bacterial initial attachment.²² The disruption or dispersal of biofilms at early stages is key since bacteria in biofilms are much more resistant to antibiotics and other antimicrobials than planktonic cells.²³ Polymeric antimicrobial coatings exploit different functionalities such as the inclusion of cationic diblock copolymers or antimicrobial polypeptides able to interact with the negatively charged cell membranes of bacteria.^{24, 25} Other possibilities include the grafting of nanoparticles and the preparation of different polymer/nanoparticle composites.²⁶⁻³⁰ Many applications of this kind have been reported for membranes with enhanced resistance to fouling and biofouling.³¹ The proposed solutions comprise the inclusion of photocatalytic nanoparticles with different structure to absorb visible light and reduce charge recombination.^{32, 33} However, up to now, the photocatalytic inactivation and antibiofilm activity of conjugated polymer nanofibers has not been explored.

In this work, we describe for the first time the photocatalytic effect of conducting polymer nanofibers (CPNs) applied for the bacterial inactivation under irradiation. To understand the utility of CPNs, two representative polymers such as poly(3,4-ethylenedioxythiophene) (PEDOT) and polyaniline (PANI) were active against the

proliferation of both gram-positive and gram-negative bacteria and avoided the formation of biofilms. These CPNs were tested in suspension and in coatings and can be used as self-cleaning materials for biomedical uses or clean surfaces in different applications.

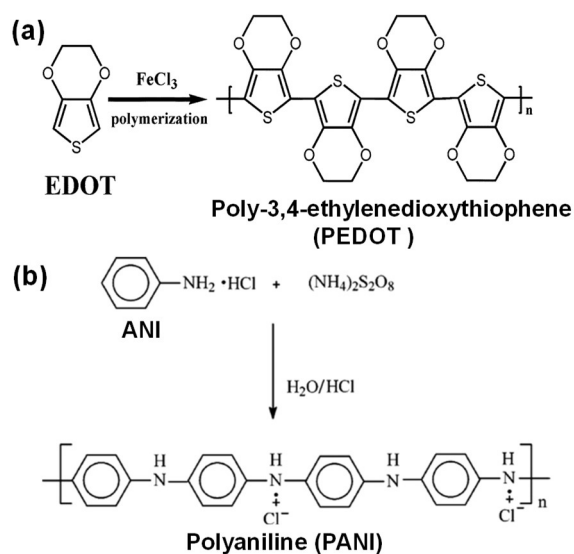
2. Experimental

2.1. Chemicals

Cetyltrimethylammonium bromide (CTAB, 98% purity), ammonium peroxydisulfate $(\text{NH}_4)_2\text{S}_2\text{O}_8$, 3,4-ethylenedioxythiophene (EDOT), aniline (ANI), and basic solvents and chemicals were obtained from Sigma-Aldrich. The chemicals used to prepare culture media were acquired from Condalab (Spain). Ultrapure water (resistivity > 18.2 M Ω , filtered through a 0.22 μm filter, particle and bacteria free) was used as solvent.

2.2. Synthesis of conjugated polymer nanostructures

The synthesis of polymer nanostructures is based on common surfactant based oxidative soft template with some modifications.³⁴ Typically, 0.015 M CTAB (cationic surfactant) was dissolved in 1 M aqueous HCl. Then, 0.025 M of ammonium persulfate (oxidant) was added into the solution as an initiator. The reaction was maintained at 5°C for 15 mins. The polymerization proceeded for 24 h after separately adding 1 M of EDOT, and ANI to the above-mentioned solution. Finally, the product was further purified with distilled water and ethanol. The structure of conducting polymer nanofibers (CPN) made of PEDOT and PANI is shown in Scheme 1. The preparation of PEDOT and PANI coatings was performed using glass coverslips (~13 mm diameter) as supports by drop casting of CPN dispersions (1 or 2 μg of PEDOT and PANI nanofibers in 1 mL of ethanol per square centimeter of surface) followed by drying for 12 h at room temperature.



Scheme 1. Chemical structure of (a) PEDOT (b) PANI polymer after chemical oxidative polymerization.

2.3. Characterization of polymer nanostructures

The CPNs prepared have been characterized by Transmission Electron Microscopy (TEM) using a Tecnai G2 30ST FEI apparatus operating at 300 kV. The morphology of the materials was investigated by Field Emission Scanning Electron Microscopy (FESEM) in a ZEISS Supra 35 equipment. The UV-visible absorption was measured in a Shimadzu UV-2450 spectrophotometer. Thermogravimetric Analysis (TGA) was carried out under argon with heating rate of $10\text{ }^{\circ}\text{C min}^{-1}$ on a thermal analyzer STA 449F, Netzsch. Nitrogen adsorption surface area measurements were carried using a Quantachrome Autosorb analyser. Pore size distribution was calculated from the desorption branch. Photocurrent measurements were performed in a Metrohm Autolab PGSTAT 30 workstation at a scanning rate of 50 mV s^{-1} using a standard three-electrode electrolytic cell with Pt foil as counter electrode. All potentials were reported against the Ag/AgCl reference electrode. Linear sweep voltammetry (LSV) scans were measured in $0.1\text{ M Na}_2\text{SO}_4$ in dark and with illumination from a UV lamp and illumination intensity of 75 mW cm^{-2} and scan rate of 20 mV s^{-1} .

2.4. Bioassays

The antimicrobial activity of PEDOT and PANI nanofibers has been studied using the strains *Escherichia coli* (CECT 516-ATCC 8739) and *Staphylococcus aureus* (CECT 240-ATCC 6538P). The microorganisms were routinely grown in 1/500 nutrient broth (NB, containing 10 g L^{-1} peptone, 5 g L^{-1} meat extract and 5 g L^{-1} NaCl, adjusted to $\text{pH } 7.0 \pm 0.1$). The antibacterial effect of CPNs was tested by inoculating suspensions with concentrations up to 1660 ng/mL with bacterial cultures containing $10^8\text{ cells mL}^{-1}$ in 24-well plates. Minimum Inhibitory Concentration (MIC) was determined by measuring colony forming units (CFU) after incubation at $37\text{ }^{\circ}\text{C}$ without stirring for 20 h. Antifouling experiments were also performed using thin coatings of PEDOT and PANI nanofibers on glass coverslips, which were placed with their functionalized surface facing up into 24-well microplates put in contact with bacterial suspensions as described before. A minimum of three replicates from at least two dilutions were used to determine CFU inhibition, which was expressed as the logarithm of CFU mL^{-1} .

Photoactivated antimicrobial activity was tested using cultures of exponentially growing bacteria, which were irradiated with a 365 nm UV-LED (LED BLS 13000-1, Mightex). The irradiance of this LED was 110.5 mW cm^{-2} and the energy delivered to CPN suspensions or coatings was calculated to mimic the amount of UV energy from solar irradiation under two scenarios described as Winter-Fall, L(+), and Summer-Spring, L(++). In both cases, the UV energy delivered was a conservative estimation representing half of the 25th

percentile of solar irradiance in the $280\text{--}400\text{ nm}$ range averaged for a period of 10 years for the latitude of Madrid, namely $1.0\text{ kW-h m}^{-2}\text{ day}^{-1}$ for L(+) and $3.0\text{ kW-h m}^{-2}\text{ day}^{-1}$ for L(++). The calculation of the insolation incident on a horizontal surface was performed using NASA's POWER project data and (<https://power.larc.nasa.gov/>). The assays were performed by irradiating during 1 h cultures grown at $37\text{ }^{\circ}\text{C}$ for 20 h. The comparison was established with cultures grown for 20 h under the same conditions without irradiation.

The metabolic activity of bacterial cells was assessed using fluorescein diacetate (FDA), which is hydrolyzed by the intracellular esterases of functional cells yielding fluorescein. For this test, PEDOT and PANI nanofibers were incubated at $25\text{ }^{\circ}\text{C}$ for 30 min with bacterial suspensions ($195\text{ }\mu\text{L}$) and $5\text{ }\mu\text{L}$ FDA (0.02% in DMSO). The fluorescence was recorded every 5 min in a Fluoroskan Ascent FL fluorometer (excitation 485 nm ; emission 528 nm). The metabolic activity of bacterial cells was also revealed using Alamar Blue stain, which is non fluorescent and reduced by active bacteria to the fluorescent compound resorufin. The method was similar with incubation at $37\text{ }^{\circ}\text{C}$ for 1 h (excitation 530 nm ; emission 590 nm). The generation of reactive oxygen species (ROS) was determined by means of 2',7'-dichlorodihydrofluorescein diacetate (H_2DCFDA), a transformation product of which, dichlorofluorescein, yields a fluorescent compound in contact with several ROS. In this case, bacterial cultures ($150\text{ }\mu\text{L}$) exposed to PEDOT and PANI were incubated with $50\text{ }\mu\text{L}$ of $10\text{ mM H}_2\text{DCFDA}$ at $25\text{ }^{\circ}\text{C}$ for 5 min (excitation 485 nm ; emission 528 nm). Cell viability was assessed using Live/Dead BacLight Bacterial Viability Assay. This is a method that stains viable cells in green using the nuclear acid stain SYTO9 and damaged cells in red by means of propidium iodide (PI). Bacteria exposed to functionalized surfaces were observed using SEM (DSM-950 Zeiss) and Confocal laser scanning microscopy (CLSM, Leica Microsystems Confocal SP5).

The cytotoxicity of PEDOT and PANI nanofibers was tested using human dermal fibroblasts (hDF) and immortal HeLa cells using the MTT (3-(4,5-dimethyl-2-thiazolyl)-2,5-diphenyl-2H-tetrazolium bromide) assay. Additionally, hemolysis assay was performed to determine the toxicity of polymer nanofibers to human red blood cells (RBCs). Additional details are provided as Supporting Information (SI).

2.5. Statistics

A one-way ANOVA coupled with Tukey's HSD (honestly significant difference) post-hoc test was performed for comparison of means. Statistically significant differences were considered to exist when $p\text{-value} < 0.05$.

3. Results and Discussion

3.1. Characterization of conducting polymer nanostructures

The morphological details of the CPNs from PEDOT and PANI used in this study as revealed by TEM and SEM micrographs are shown in Fig. 1a-d. The average diameter of PEDOT and PANI nanofibers was about 40 nm with a length of several microns.

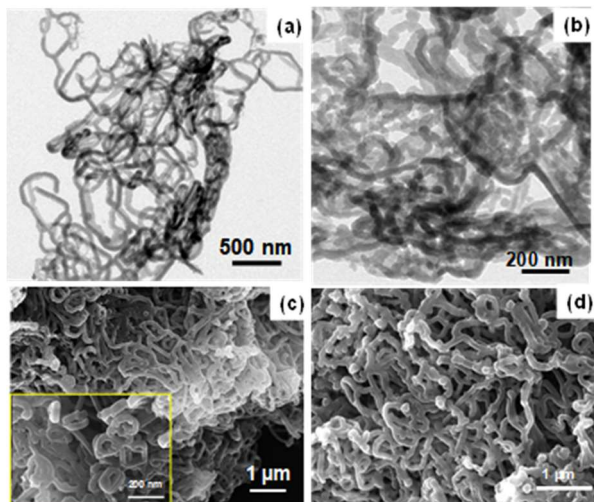


Figure 1. (a, b) TEM micrographs of PEDOT and PANI. SEM micrographs of (c) PEDOT (inset: high magnification image) and (d) PANI.

FTIR analysis has been carried out to investigate the chemical structures of PEDOT and PANI (Fig.S1, SI). The peaks around 1360 and 1480 cm^{-1} , due to C-C and C=C stretching of the quinoidal structure of the thiophene ring, indicated the formation of PEDOT. The major bands at 1564 and 1496 cm^{-1} that appeared in the spectrum of PANI due to the C=C stretching vibrations of a quinoid ring and a benzenoid ring (a quinoid ring and a benzenoid ring are the basic molecular units of PANI), respectively. The bands at 1295 and 1212 cm^{-1} belong to the C-N and C=N stretching mode, respectively. The molar mass of PEDOT and PANI polymers have been found to be 1205 and 980 g mol^{-1} , as determined by gel permeation chromatography (Table S1, SI). TGA analyses (Fig. S2, SI) showed high thermal stability of both polymers in comparison to other common conducting polymers, such as polypyrrole, which is consistent with earlier reports.³⁵ A three stages of decomposition pattern have been obtained for PEDOT nanofibers with 50 % weight loss around 430 °C, while PANI decomposed less than 40 % even at higher temperature, ~551 °C. Initial weight losses can be attributed to the loss of water molecules and low molecular weight oligomers. BET measurements indicated mesoporosity of both polymers with type IV nitrogen adsorption-desorption isotherms (Fig. S3, SI). PEDOT displayed higher surface area (11.5 $\text{m}^2 \text{g}^{-1}$) and

pore volume (0.016 $\text{cm}^3 \text{g}^{-1} \text{nm}^{-1}$) than PANI nanofibers (6.6 $\text{m}^2 \text{g}^{-1}$ and 0.001 $\text{cm}^3 \text{g}^{-1} \text{nm}^{-1}$, respectively) along with a broader pore size distribution, in the 3–90 nm range.

The spectral properties and electrochemical response of PEDOT and PANI nanofibers are shown in Fig. 2. As depicted in Fig. 2a, an absorption band around 354 nm was observed for PEDOT nanofibers along with a broad band centered about 980 nm in the near IR region that can be attributed to oligomers. LSV scans showed strong photo response under UV light with high current density of 4.1 mA cm^{-2} at 0.8 V (0.035 mA cm^{-2} under dark) as shown in Fig. 2b. This observation is consistent with the stable photoresponse observed under repeated on-off as shown in Fig. 2c. Fig. 2d displays the UV-visible spectra of the PANI, with a strong peak at 380 nm and a long tail that may be attributed to the $\pi-\pi^*$ transition. The photoresponse of PANI was similar than that of PEDOT, but with less photocurrent (0.41 mA cm^{-2} at 0.8 V) (Fig.2e, f).

PEDOT and PANI nanofibers displayed high positive surface charge with zeta potential of +39.5 mV and +41.8 mV respectively at pH 7, which stabilize their water suspensions by means of electrostatic forces preventing further aggregation. The high positive surface charge is expected to interact with the components of bacterial envelopes, namely peptidoglycans and lipopolysaccharides (*E. coli*) from gram positive (*S. aureus*) and gram negative (*E. coli*) bacteria, respectively.

3.2. Photocatalytic assays

The antimicrobial activity of photoexcited CPNs consisting of PEDOT and PANI nanofibers has been tested against growing cultures of *S. aureus* and *E. coli*. Even when positively charged polymers, including PANI and PEDOT are considered biocidal, the effect is weak and to approach practical applications, they require the synergistic combination with other antimicrobials.³⁶ In our study, PEDOT made more difficult the growth of *S. aureus* but bacterial growth was still positive as shown in Fig. 3a. After 20 h in contact with cultures starting with 10^8 CFU mL^{-1} , the total number of CFU was still increasing at the highest tested concentration of PEDOT. The light-induced growth impairment caused by PEDOT CPNs is clear from Figs. 3a-b. Light fluxes mimicking Winter-Fall, L (+) (1.0 $\text{kW-h m}^{-2} \text{day}^{-1}$) and Summer-Spring L(++) (3.0 $\text{kW-h m}^{-2} \text{day}^{-1}$) solar irradiation resulted in a ~4-log decrease (99.99 %) of the capacity of cells to establish new colonies at CPN concentration of 883 ng mL^{-1} for L(+) and no viable colonies at all for L(++). This means an outstanding > 10-log decrease in the formation of

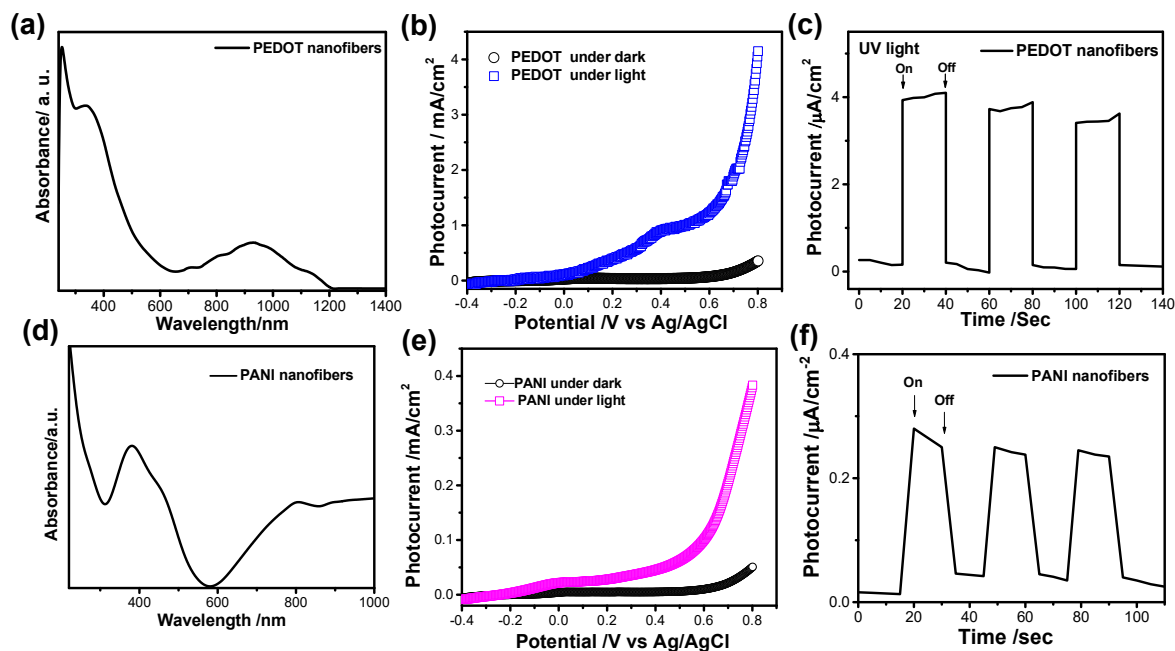


Figure 2. (a) UV-visible spectrum of PEDOT nanofibers. (b) LSV scans for PEDOT. (c) Photocurrent response of PEDOT under UV light. (d) UV-vis spectrum of PANI nanofibers. (e) LSV scans for PANI nanofibers. (f) Photocurrent response of PANI under UV light.

new colonies for that dose with respect to controls. The effect (Fig. 3b) was lower when studying cell metabolic activity by means of FDA tests, which can be ascribed to the existence of viable but non-culturable cells with metabolic activity but failing to establish new colonies.³⁷

The light-induced redox mechanism of CPNs antimicrobial action was studied using H₂DCFDA to demonstrate the role of ROS. The quantitative data

showed significant increase in ROS for cells exposed both to light and PEDOT nanofibers, particularly for the L(++) scenario (Fig. 4c). This is consistent with the alignment of CPNs band-edge state with oxygen reduction potential, which could favor the formation of superoxide radicals (O₂⁻).³⁸ It is well documented that when intracellular ROS such as O₂⁻, hydrogen peroxide, and hydroxyl radical reach a threshold, the structure and activity of proteins and key enzymatic routes become affected, finally causing cell death.³⁹

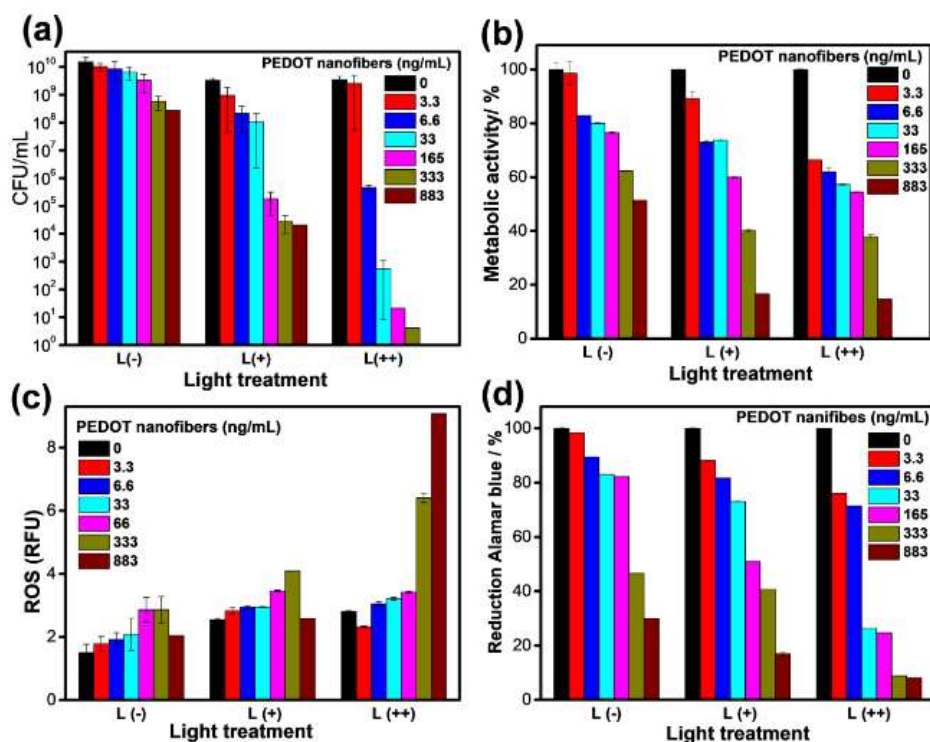


Figure 3. (a) Colony forming units mL⁻¹; (b) metabolic activity by FDA assay; (c) ROS in Relative Fluorescence Units (RFU); (d) Alamar blue viability assay. Results for *S. aureus* cultures in contact with PEDOT nanofibers.

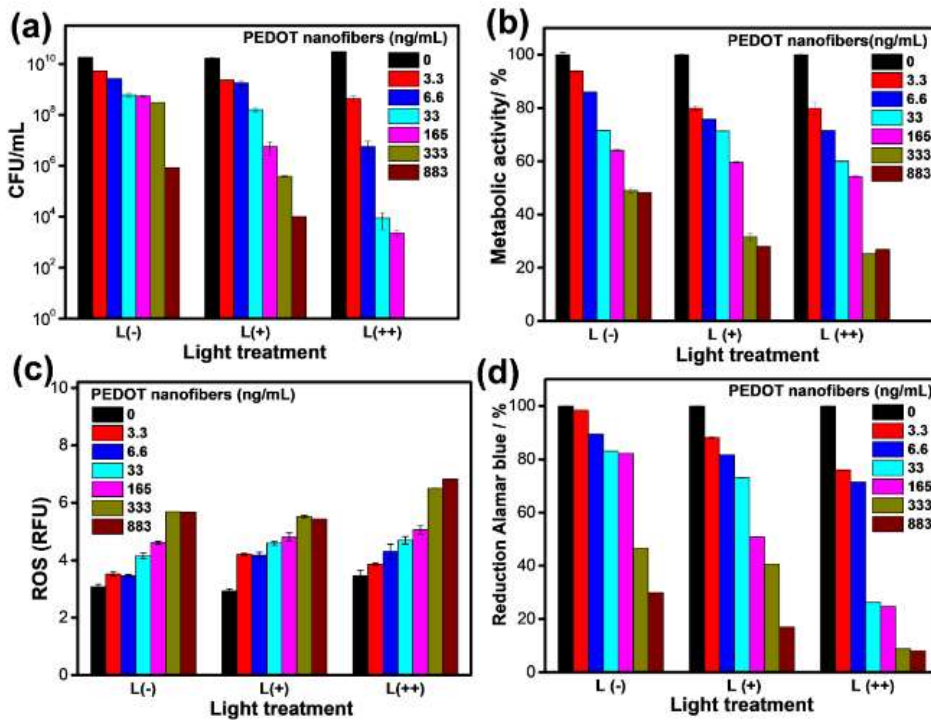


Figure 4. (a) Colony forming units mL^{-1} ; (b) metabolic activity by FDA assay; (c) ROS in Relative Fluorescence Units (RFU); (d) Alamar blue viability assay. Results for *E. coli* cultures in contact with PEDOT nanofibers.

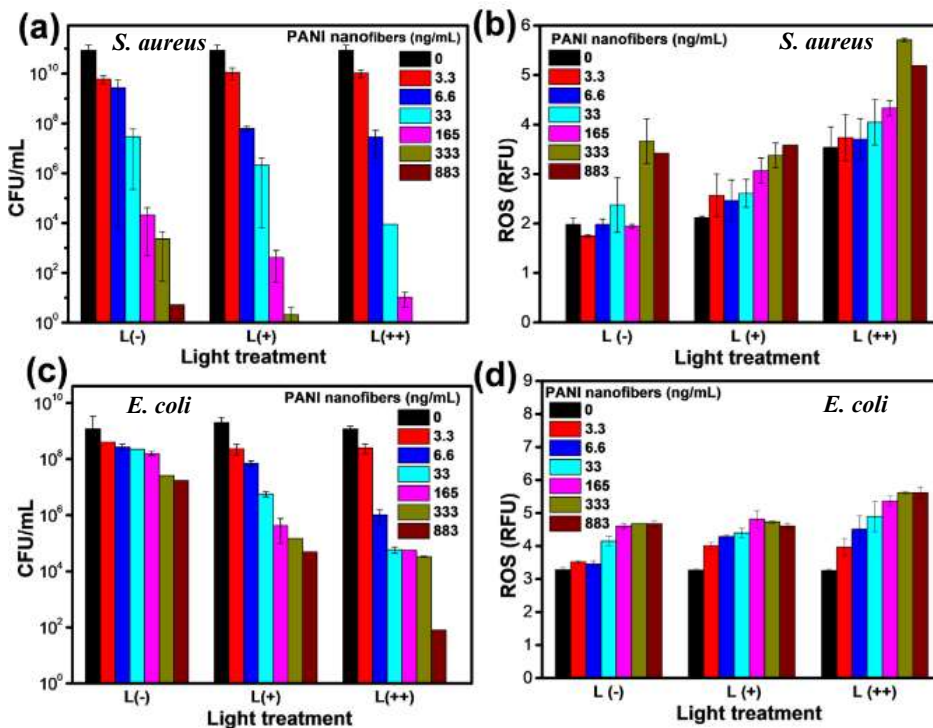


Figure 5. Colony forming units mL^{-1} and ROS production in Relative Fluorescence Units (RFU) of cultures of *S. aureus* (a and b) and *E. coli* (c and d) in contact with suspensions of PANI nanofibers.

Further, Alamar Blue assay lead to > 80 % reduction in metabolic activity in the presence of > 33 ng/mL PEDOT nanofibers and > 90 % reduction for > 333 ng/mL under irradiation whereas the same concentration in dark on conditions, only led to < 20 % decrease (Fig. 4d).

The inactivation of the gram-negative *E. coli* with PEDOT nanofibers was also studied as shown in

Fig. 4. A substantial reduction in colony forming units of *E. coli* was detected under light irradiation leading to a complete absence of CFU for 333 ng/mL and higher concentration (Fig. 4a). This observation agreed with a significant reduction of metabolic activity of around 80 % as shown in Fig. 4b. Compared to *S. aureus*, less ROS generation was observed for *E. coli*. although metabolic

impairment also reached > 90 % reduction for concentrations of PEDOT > 333 ng/mL (Fig. 4d).

CPNs from PANI nanofibers were also tested against bacterial cells displaying significant anti-bacterial effect against both *S. aureus* and *E. coli*. Fig. 5 represents the viability and ROS generation with respect to the control under light irradiation. The overall results showed that PANI exhibited better photocatalytic for *S. aureus* than *E. coli*. Fig. 5 shows complete disappearance of *S. aureus* CFU at 333 ng/mL with clear increase in ROS generation, which was comparable with the effect obtained with PEDOT nanofibers. Relatively higher concentration was required to completely inhibit *E. coli* growth in comparison with PEDOT nanofibers, although the effect of light irradiation was also clear with differences reaching four orders of magnitude when comparing L(-) and L(++) for the higher concentrations of CPNs. The results are consistent with the band gaps of PANI and PEDOT, PANI, which are able to generate

electron-hole pairs under light irradiation yielding ROS.^{40, 41} The differences in the structure of the external envelopes of gram-positive and gram-negative bacteria explain the different extent of cell impairment. *E. coli* is a gram-negative bacterium protected by an external outer membrane, while *S. aureus* has no outer membrane, but a thick peptidoglycan layer. The destabilization of the peptidoglycan layer leads to a rapid cell impairment, which can be explained because gram-positive bacteria are more prone to interact with positively charged surfaces because of their larger fraction of anionic membrane phospholipids.^{42, 43}

Further, the EDOT and ANI monomers were polymerized without using the surfactant based soft template to give bulk PEDOT and PANI to be used as control and compare their activity with the one shown by the polymer nanofibers. Fig. S4 shows the corresponding SEM indicating the formation of highly aggregated micrometer-size bulk PEDOT and PANI. The photocatalytic inactivation of

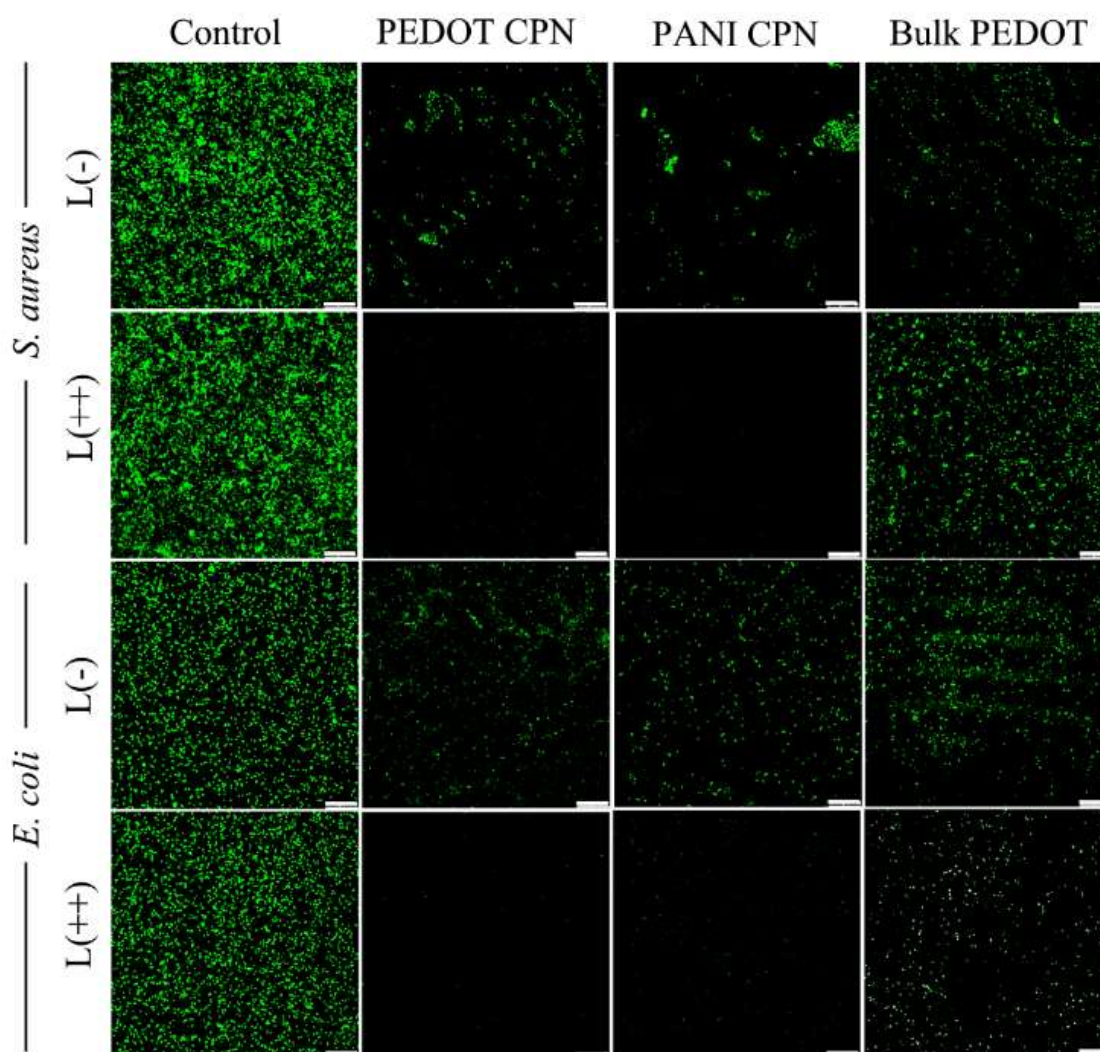


Figure 6. Live/Dead confocal micrographs of *S. aureus* (upper rows) and *E. coli* (lower rows) cultures on control glass surface and glass functionalized with PEDOT and PANI CPNs and bulk PEDOT after 20 h in darkness and 19h in darkness followed by 1 h irradiation, labelled as L(-) and L(++). (Surface density 2 $\mu\text{g}/\text{cm}^2$; the scale bar represents 50 μm .)

bacteria using bulk PEDOT and PANI was evaluated under the same irradiation conditions and results shown in Fig.S5. Bulk PEDOT displayed very low photocatalytic inactivation of both *S. aureus* and *E. coli*, with still ~80% and ~60% of cells remaining viable after treatment, respectively. Similar results were observed for bulk PANI. These results contrast with the high activity of CPNs from PEDOT and PANI and highlight the role of polymer nanofibers on the photocatalytic inactivation of bacteria.

Antifouling experiments were performed by dispersing PEDOT and PANI on glass coverslips with a surface density of CPN of 2 $\mu\text{g}/\text{cm}^2$. The as-prepared functionalized surfaces were exposed to bacterial cultures with and without irradiation and the results visualized using confocal micrographs as shown in Fig. 6, which corresponds to the integrity of cell membranes as stained by the Live/Dead bacterial viability combination of dyes. Fig. 6 shows control cultures with numerous green-stained viable cells and cultures exposed to CPNs. Irradiated cultures exposed PEDOT and PANI nanofibers were essentially free of viable bacteria. Non-irradiated CPNs were considerably less colonized than control glass substrate, but still showed a considerable number of green-stained viable cells on their surface, and the same for bulk PEDOT. Few red-marked, membrane-damaged cells were observed, probably meaning that they become detached from the surface before staining. Clearly, bulk PEDOT induce a much lower level of bacterial cell damage even under light irradiation confirming that CNP structure is essential for exerting a high damage to bacterial cells.

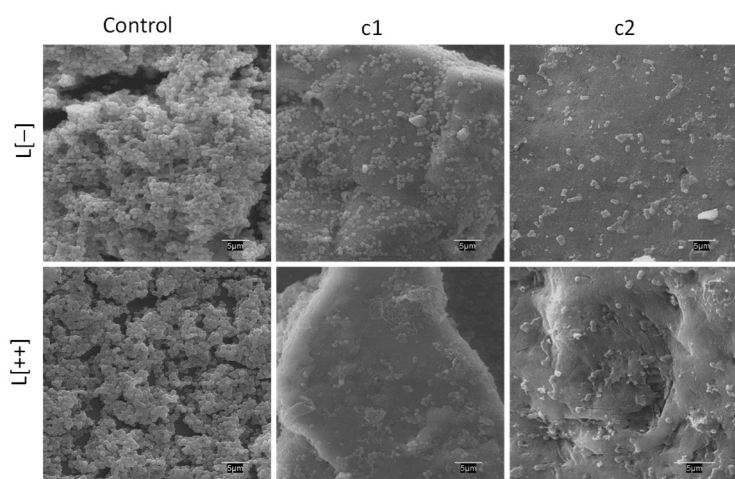


Figure 7. SEM micrographs of *S. aureus* biofilms on glass surface (control) and PEDOT-functionalized glass after contact with cultures for 20 h in darkness L(-), and 20 h in darkness followed by 1h UV irradiation, L(++). (c1 and c2 represent surface densities of 1 and 2 $\mu\text{g}/\text{cm}^2$; the scale bar represents 5 μm .)

SEM micrographs also support the phototoxicity results of the CPN functionalized surfaces. Figs. 7

and 8 show that *E. coli* and *S. aureus* not exposed to CPNs retained their morphology with intact cell membranes. Bacterial adhesion structures were clear and still visible for non-irradiated functionalized surfaces. For PEDOT in irradiated surfaces nearly no bacteria were found colonizing the surface. SEM images also indicated that polymer nanofibers caused cell membrane crimping and lysis in presence of light. This toxicity may probably be caused by the combined effect of the physical interaction between the polymer nanofibers and the bacterial envelopes and the generation of light-induced ROS. The production of ROS by CPNs would be favored by their large surface area, with more reactive sites and stronger light absorption. In fact, growth inhibition of the cells has been attributed to the bacterial attachment modes of CPN through electrostatic surface complexation or intercalation that induced cell wall alteration.

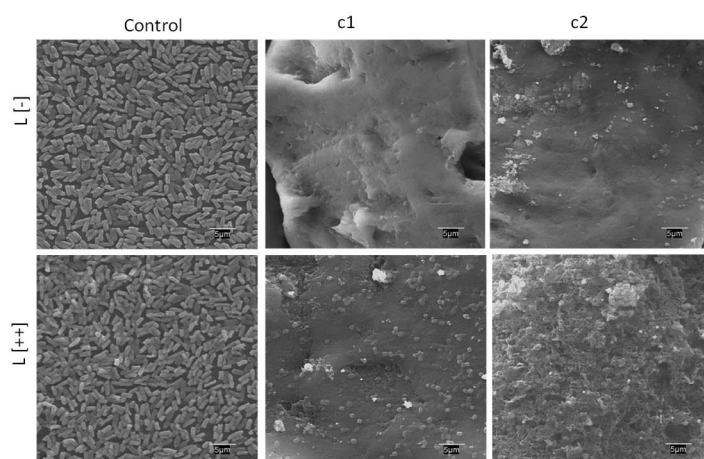


Figure 8. SEM micrographs of *E. coli* biofilms on glass surface (control) and PEDOT-functionalized glass after contact with cultures for 20 h in darkness L(-), and 20 h in darkness followed by 1h UV irradiation, L(++). (c1 and c2 represent surface densities of 1 and 2 $\mu\text{g}/\text{cm}^2$; the scale bar represents 5 μm).

3.3. Biocompatibility tests

Finally, we assessed the biocompatibility and cytotoxicity of CPNs to hDF and HeLa cells using the MTT cell viability assay. Fig. 9 shows that viability kept > 95 % for hDF cells at the highest tested concentration (3330 ng/mL) for PEDOT and PANI nanofibers. On the contrary, significant effect, with ~50 % reduction in viability of HeLa cells was observed (Fig. 9a-b and d-e). Additionally, *in vitro* hemolysis data showed limited toxic effect (< 10 % or > 90 % cells undamaged) to red blood cells measured by hemoglobin release after contact with CPNs (Fig. 9c-f). The results showed good biocompatibility and absence of acute toxicity both for PEDOT and PANI nanofibers and suggest that their biomedical use is possible for applications such as topic antimicrobials of wound dressings.

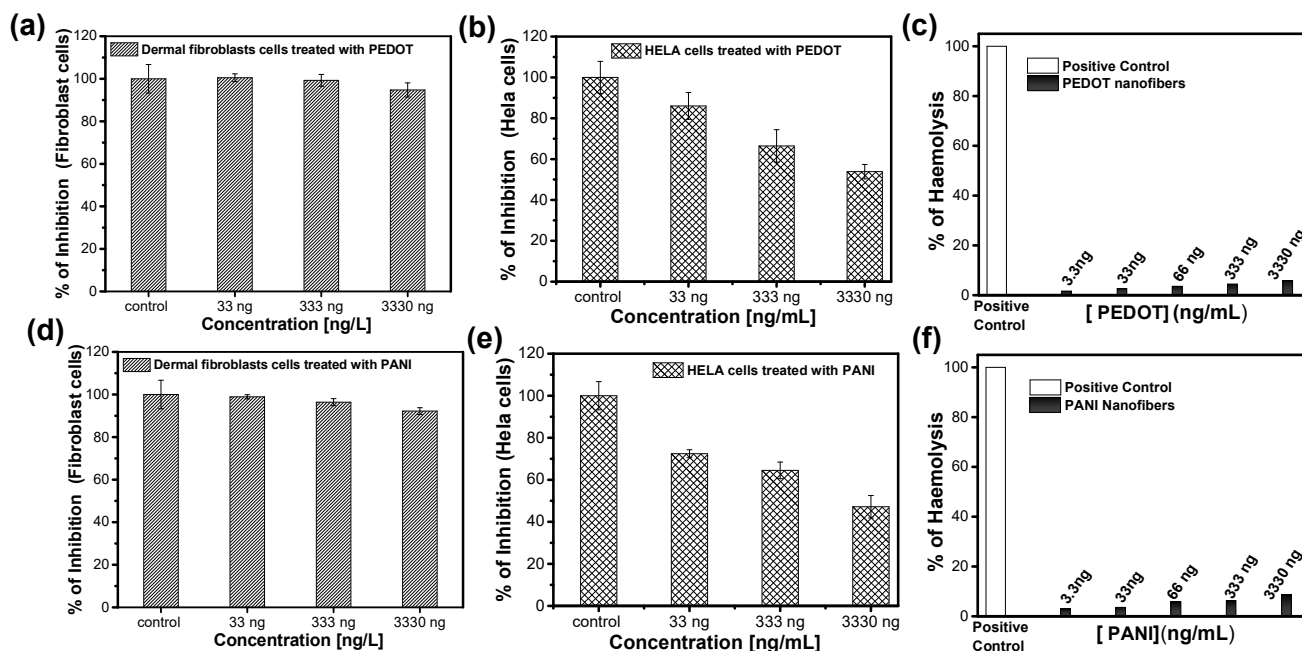


Figure 9. Results of cell viability using MTT assay for (a) hDF and (b) HeLa cells after 24-hours in contact with PEDOT nanofibers. (c) Hemolysis assay for PEDOT nanofibers and Triton-X used as a positive control. Results of cell viability using MTT assay for (d) hDF and (e) HeLa cells in contact with PANI nanofibers. (f) Hemolysis assay for PANI nanofibers. (Data are shown as mean \pm standard deviation of three independent experiments.)

4. Conclusions

Herein, conjugated polymeric nanostructures (CPNs) are reported as photoactive antimicrobials against gram-positive and gram-negative bacteria. PEDOT and PANI nanofibers displayed high antimicrobial effect when irradiated with 365 nm light in doses similar or lower than the UVA component of solar radiation. The bactericidal effect is due to the production of ROS under light irradiation, which resulted in effective inhibition of the bacteria *S. aureus* and *E. coli*. The bactericidal activity was directly related to the nanofibrous structure of CPN materials as evidenced by the lack of bacterial growth inhibition in contact with bulk polymers. The enhanced biocidal activity of polymer nanofibers was attributed to their high surface area and light absorption. Coatings prepared by drop casting of PEDOT and PANI CPNs demonstrated excellent antimicrobial activity with surfaces essentially free of bacteria even after prolonged exposure in dark to exponentially growing cultures in an appropriate culture medium. Functionalized surfaces inhibited the formation of biofilms. The concentrations of CPNs required for photoinduced biocidal activity are below the microgram per milliliter range. Both PEDOT and PANI CPNs showed excellent biocompatibility evidenced by the absence of toxicity to human fibroblasts and red blood cells.

Acknowledgements

The authors acknowledge the funding provided by the European Union's Horizon 2020 research and

innovation programme under the Marie Skłodowska-Curie grant agreement No 754382, GOT ENERGY TALENT, Spanish Government (CTM2016-74927-C2-1/2-R and RTI2018-094840-B-C31) and the University of Alcalá (CCG19/CC-037).

References

1. Q. Cui, X. Wang, Y. Yang, S. Li, L. Li, S. Wang, Binding-directed energy transfer of conjugated polymer materials for dual-color imaging of cell membrane. *Chem. Mater.* 2016, **28**, 4661-4669.
2. J. G. Ibanez, M. E. Rincón, S. Gutierrez-Granados, M. Chahma, O. A. Jaramillo-Quintero, B. A. Frontana-Urbe Conducting polymers in the fields of energy, environmental remediation, and chemical-chiral Sensors. *Chem. Rev.* 2018, **118**, 4731-4816.
3. C. Zhao, Z. Chen, R. Shi, X. Yang, T. Zhang, Conjugated polymer nanoparticles for imaging, cell activity regulation, and therapy. *Adv. Funct. Mater.* 2019, **29**, 1806818.
4. S. Ghosh, M. Thandavarayan, R. N. Basu, Nanostructured conducting polymers for energy applications: towards a sustainable platform. *Nanoscale* 2016, **8**, 6921-6947.
5. D. Tuncel, π -Conjugated nanostructured materials: preparation, properties and photonic applications. *Nanoscale Adv.* 2019, **1**, 19-33.
6. X. Yuan, D. Floresyona, P.-H. Aubert, T. -T. Bui, S. Remita, S. Ghosh, F. Brisset, F. Goubard, H. Remita, Photocatalytic Degradation of Organic Pollutant with

- Polypyrrole Nanostructures under UV and Visible light, *Appl. Catal. B: Environ.* 2018, **242**, 284–292.
- 7.C. Dai, B. Liu, Conjugated polymers for visible-light-driven photocatalysis. *Energy Environ. Sci.* 2020, **13**, 24–52.
- 8.C. Dai, Y. Pan, B. Liu, Conjugated Polymer Nanomaterials for Solar Water Splitting. *Adv. Energy Mater.* 2020, **10**, 2002474.
- 9.C. Zhao, Z. Chen, R. Shi, X. Yang, T. Zhang, Recent advances in conjugated polymers for visible-light-driven water splitting. *Adv. Mater.* 2020, **32**, 1907296.
- 10.T. Senthilkumar, L. Zhou, Q. Gu, L. Liu, F. Lv, S. Wang, Conjugated polymer nanoparticles with appended photo-responsive units for controlled drug delivery, release, and imaging. *Angew. Chem. Int. Ed.* 2018, **57**, 13114–13119.
11. J. -G. Wu, J.-H. Chen, K.-T. Liu, S.-C. Luo, Engineering antifouling conducting polymers for modern biomedical applications. *ACS Appl. Mater. Interfaces* 2019, **11**, 21294–21307.
- 12.L. Ma, S. Jayachandran, Z. Li, Z. Song, W. Wang, X. Luo, Antifouling and conducting PEDOT derivative grafted with polyglycerol for highly sensitive electrochemical protein detection in complex biological media. *J. Electroanal. Chem.* 2019, **840**, 272–278.
- 13.T. Goda, Y. Miyahara, Electrodeposition of zwitterionic PEDOT films for conducting and antifouling surfaces. *Langmuir* 2019, **35**, 1126–1133.
- 14.X. Liang, M. Sun, L. Li, R. Qiao, K. Chen, Q. Xiao, F. Xu, Preparation and antibacterial activities of polyaniline/Cu_{0.05}Zn_{0.95}O nanocomposites. *Dalton Trans.* 2012, **41**, 2804–2811.
- 15.Z. Kucekova, P. Humpolicek, V. Kasparkova, T. Perecko, M. Lehocký, I. Hauerlandová, P. Saha, J. Stejskal, Colloidal polyaniline dispersions: Antibacterial activity, cytotoxicity and neutrophil oxidative burst. *Colloids Surf. B* 2014, **116**, 411–417.
16. M. R. Gizdavic-Nikolaidis, J. R. Bennett, S. Swift, A. J. Easteal, M. Ambrose, Broad spectrum antimicrobial activity of functionalized polyanilines. *Acta Biomater.* 2011, **7**, 4204–4209.
- 17.U. Bogdanović, V. Vodnik, M. Mitrić, S. Dimitrijević, S. D. Škapin, V. Žunič, M. Budimir, M. Stoiljković, Nanomaterial with high antimicrobial efficacy-copper/polyaniline nanocomposite. *ACS Appl. Mater. Interfaces* 2015, **7**, 1955–1966.
- 18.P. Boomi, H. G. Prabu, Synthesis, characterization and antibacterial analysis of polyaniline/Au–Pd nanocomposite. *Colloids Surf. A* 2013, **429**, 51–59.
- 19.C. J. Jeong, S. M. Sharkar, I. In, S. Y. Park, Iron oxide@PEDOT-based recyclable photothermal nanoparticles with poly(vinylpyrrolidone) sulfobetaines for rapid and effective antibacterial activity. *ACS Appl. Mater. Interfaces* 2015, **7**, 9469–9478.
20. A. M. Kumar, A. Y. Adesina, M. A. Hussein, S. Ramakrishna, N. Al-Aqeeli, S. Akhtar, S. Saravanan, PEDOT/FHA nanocomposite coatings on newly developed Ti-Nb-Zr implants: Biocompatibility and surface protection against corrosion and bacterial infections. *Mater. Sci. Eng. C* 2019, **98**, 482–495.
- 21.A. Kumar, A. Alam, M. Rani, N. Z. Ehtesham, S. E. Hasnain, Biofilms: Survival and defense strategy for pathogens. *Int. J. Med. Microbiol.* 2017, **307**, 481–489.
22. Z. K. Zander, M. L. Becker, Antimicrobial and antifouling strategies for polymeric medical devices. *ACS Macro Letters* 2018, **7**, 16–25.
- 23.D. Sharma, L. Misba, A. U. Khan, Antibiotics versus biofilm: an emerging battleground in microbial communities. *Antimicrob. Resist. Infect. Control* 2019, **8**, 76.
24. X. Ding, C. Yang, T. P. Lim, L. Y. Hsu, A. C. Engler, J. L. Hedrick, Y.-Y. Yang, Antibacterial and antifouling catheter coatings using surface grafted PEG-b-cationic polycarbonate diblock copolymers. *Biomaterials* 2012, **33**, 6593–6603.
25. Q. Gao, P. Li, H. Zhao, Y. Chen, L. Jiang, P. X. Ma, Methacrylate-ended polypeptides and polypeptoids for antimicrobial and antifouling coatings. *Polym Chem.* 2017, **8**, 6386–6397.
- 26.Y. Boguslavsky, M. Shemesh, A. Friedlander, R. Rutenberg, A. M. Filossof, A. Buslovich, E. Poverenov, Eliminating the need for biocidal agents in anti-biofouling polymers by applying grafted nanosilica instead. *ACS Omega* 2018, **3**, 12437–12445.
27. R. Namivandi-Zangeneh, E. H. H. Wong, C. Boyer, Synthetic Antimicrobial Polymers in Combination Therapy: Tackling Antibiotic Resistance. *ACS Infect. Dis.* 2021, **2**, 215–253.
28. T.-K. Nguyen, S. J. Lam, K. K. K. Ho, N. Kumar, G. G. Q. Ocid, S. Egan, C. Boyer, E. H. H. Wong, Rational Design of Single-Chain Polymeric Nanoparticles That Kill Planktonic and Biofilm Bacteria. *ACS Infect. Dis.* 2017, **3**, 237–248.
29. S. Fazli-Shokouhi, F. Nasirpouri, M. Khatamian, Polyaniline-modified graphene oxide nanocomposites in epoxy coatings for enhancing the anticorrosion and antifouling properties. *J. Coat. Technol. Res.* 2019, **16**, 983–997.
30. S. Wen, P. Wang, L. Wang, Preparation and antifouling performance evaluation of fluorine-containing amphiphilic silica nanoparticles. *Colloids Surf. A* 2020, 125823.
31. S. Zhao, Z. Liao, A. Fane, J. Li, C. Tang, C. Zheng, J. Lin, L. Kong, Engineering antifouling reverse

osmosis membranes: A review. *Desalination* 2021, **499**, 114857.

PET-RAFT for Photodynamic Inactivation of Bacteria. *Macro Rapid Comm.* 2021, 2100106.

32. T. Sun, Y. Liu, L. Shen, Y. Xu, R. Li, L. Huang, H. Lin, Magnetic field assisted arrangement of photocatalytic TiO₂ particles on membrane surface to enhance membrane antifouling performance for water treatment. *J. Colloid Interface Sci.* 2020, **570**, 273-285.

33. L. Zhang, J. Sha, R. Chen, Q. Liu, J. Liu, J. Yu, H. Zhang, C. Lin, J. Wang, Three-dimensional flower-like shaped Bi₅O₇I particles incorporation zwitterionic fluorinated polymers with synergistic hydration-photocatalytic for enhanced marine antifouling performance. *J. Hazard. Mater.* 2020, **389**, 121854.

34. S. Ghosh, A. K. Mallik, R. N. Basu, Enhanced photocatalytic activity and photoresponse of poly(3,4-ethylenedioxythiophene) nanofibers decorated with gold nanoparticle under visible light. *Solar Energy* 2018, **159**, 548-560.

35. S. Ghosh, S. Bera, S. Bysakh, R. N. Basu, Highly active multimetallic palladium nanoalloys embedded in conducting polymer as anode catalyst for electrooxidation of ethanol. *ACS Appl. Mater. Interfaces* 2017, **9**, 33775-33790.

36. Q. Jia, S. Shan, L. Jiang, Y. Lang, D. Li, Synergistic antimicrobial effects of polyaniline combined with silver nanoparticles. *J. Appl. Polym. Sci.* 2012, **125**, 3560-3566.

37. D. Venieri, E. Chatzisyneon, M. S. Gonzalo, R. Rosal, D. Mantzavinos, Inactivation of *Enterococcus faecalis* by TiO₂-mediated UV and solar irradiation in water and wastewater: culture techniques never say the whole truth. *Photochem. Photobiol. Sci.* 2011, **10**, 1744-1750.

38. S. Ghosh, N. A. Kouame, L. Ramos, S. Remita, A. Dazzi, A. Deniset-Besseau, P. Beaunier, F. Goubard, P. -H. Aubert, H. Remita, Conducting polymer nanostructures for photocatalysis under visible light. *Nat. Mater.* 2015, **14**, 505-511.

39. B. Ezraty, A. Gennaris, F. Barras, J.-F. Collet, Oxidative stress, protein damage and repair in bacteria. *Nat. Rev. Microbiol.* 2017, **15**, 385.

40. O. Kwon, M. L. McKee, Calculations of band gaps in polyaniline from theoretical studies of oligomers. *J. Phys. Chem. B* 2000, **104**, 1686-1694.

41. C. Gravalidis, A. Laskarakis, S. Logothetidis, Fine tuning of PEDOT electronic properties using solvents. *Eur. Phys. J. Appl. Phys.* 2009, **46**, 12505.

42. N. Malanovic, K. Lohner, Gram-positive bacterial cell envelopes: The impact on the activity of antimicrobial peptides. *Biochim. Biophys. Acta Biomembranes* 2016, **1858**, 936-946.

43. G. Ng, P. Judzewitsch, M. Li, C. W. Pester, K. Jung, C. Boyer, Synthesis of Polymer Brushes Via SI-

Supporting Information

Conjugated polymer nanostructures displaying high photoactivated antimicrobial and antibiofilm functionalities

Srabanti Ghosh,^{1,3*} Georgiana Amariei,² Marta E. G. Mosquera,^{1*} and Roberto Rosal²

¹ Department of Organic and Inorganic Chemistry, Institute of Chemical Research “Andrés M. del Río” (IQAR), Universidad de Alcalá, 28805 Alcalá de Henares, Madrid, Spain

² Department of Chemical Engineering, Universidad de Alcalá, 28805 Alcalá de Henares, Madrid, Spain

³ Energy Materials & Devices Division, CSIR-Central Glass and Ceramic Research Institute, Kolkata-700032, India

Corresponding authors:

Dr. Marta E. G. Mosquera: martaeg.mosquera@uah.es

Dr. Srabanti Ghosh: srabanti.ghosh@uah.es

CONTENTS:

Additional details on cytotoxicity tests

Figure S1. TGA profiles of (a) PEDOT and (b) PANI nanofibers.

Figure S2. Nitrogen adsorption and desorption isotherms measured at 77 K and pore radius distributions of (a, b) PEDOT and (c, d) PANI nanofibers.

Figure S3. SEM images of bulk PEDOT and bulk PANI obtained from the monomer solution in presence of oxidant without using any surfactant or soft template.

Figure S4. Colony forming units mL⁻¹ of *S. aureus* and *E. coli* cultures in contact with suspensions of (a, b) bulk PEDOT and (c) bulk PANI.

Additional details on cytotoxicity tests

Cells were harvested from culture flasks by trypsinization and aliquots of 100 μL seeded in 96-well microplates in densities of 1×10^4 cells per well and incubated for 24 h at 37 $^\circ\text{C}$ in a humidified atmosphere of 5% CO_2 in air (approx. 70-80% confluence). Cell toxicity was studied by means of the colorimetric MTT (3-(4,5-dimethyl-2-thiazolyl)-2,5-diphenyl-2H-tetrazolium bromide) assay based on the reduction of tetrazolium salt by the mitochondrial dehydrogenases of viable cells to yield formazan as colored insoluble product. The reduction of absorbance can be attributed to a lower number of viable cells or the inhibition of cell proliferation upon exposure to PEDOT and PANI nanofibers. Stock solutions of PEDOT and PANI nanofibers were prepared in PBS, diluted in MEM media and dispensed into wells. After 24 h exposure, PEDOT and PANI nanofibers were removed, replaced with MEM/MTT mixture and incubated for 4 h. After that, formazan crystals were dissolved in DMSO and absorbance recorded at 570 and 630 nm using a BioTek[®] Elisa Reader. At least two independent runs with at least three replicas were used for each concentration level. Cell viability was derived from the formazan generated, the amount of which is proportional to the number of metabolically active cells. Untreated cells and media alone were taken as positive and negative controls. The number of surviving cells was expressed as percent viability and calculated as follows:

$$\text{Percent viability of cells} = \frac{\text{the absorbance of the sample (treated cells)} - \text{background}}{\text{the absorbance of the control (untreated cells)} - \text{background}} \times 100 \quad (1)$$

For the hemolysis assay, erythrocytes obtained from blood cells were PBS washed (pH 7.2) and resuspended in PBS. Then 100 μL of the erythrocyte solution were incubated with PEDOT and PANI nanofibers for 2 h in 96-well plates with PBS. Intact erythrocytes were pelleted by centrifugation at $1000 \times g$ for 5 min at 4 $^\circ\text{C}$ and the release of hemoglobin was measured using UV-Vis absorbance at 450 nm. The negative and positive controls were PBS and control 1% TritonX-100, respectively. The percent of hemolysis was calculated as follows:

$$\text{Hemolysis \%} = \frac{(\text{sample absorbance} - \text{negative control})}{(\text{positive control} - \text{negative control})} \times 100\% \quad (2)$$

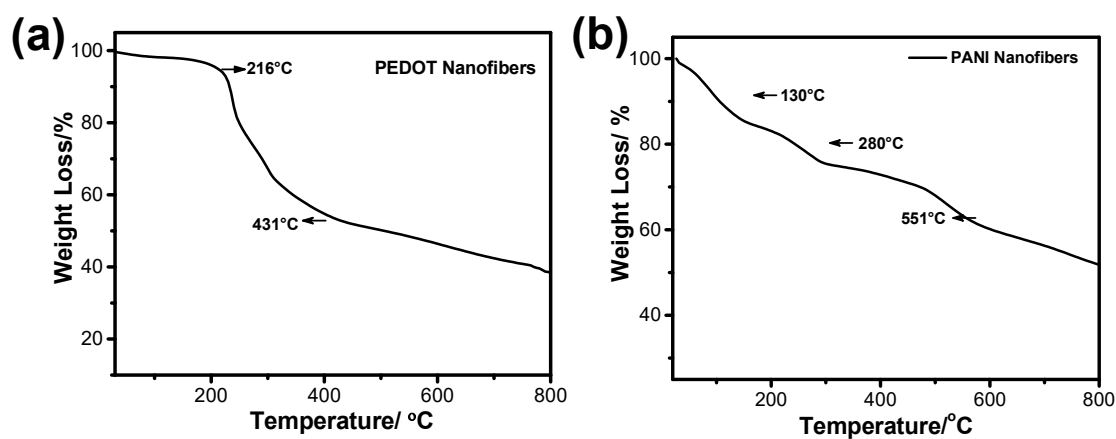


Figure S1. TGA profiles of (a) PEDOT and (b) PANI nanofibers.

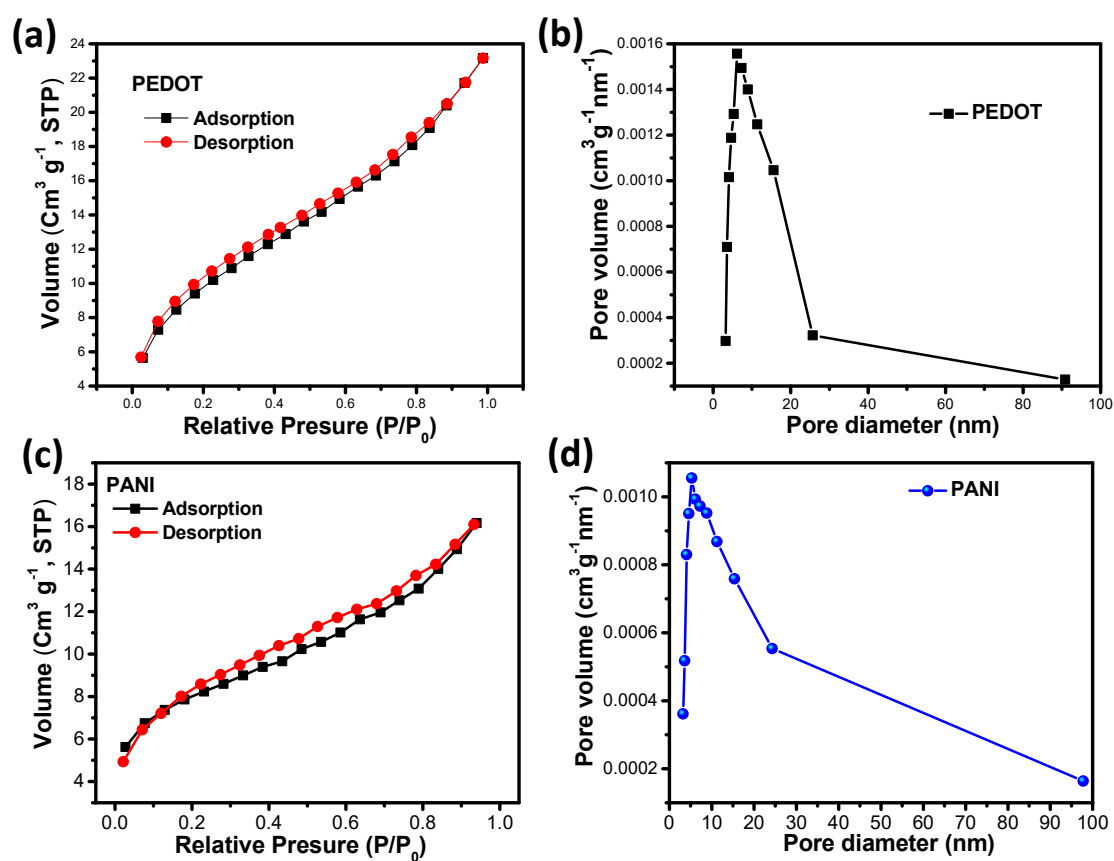


Figure S2. Nitrogen adsorption and desorption isotherms measured at 77 K and pore radius distributions of (a, b) PEDOT and (c, d) PANI nanofibers.

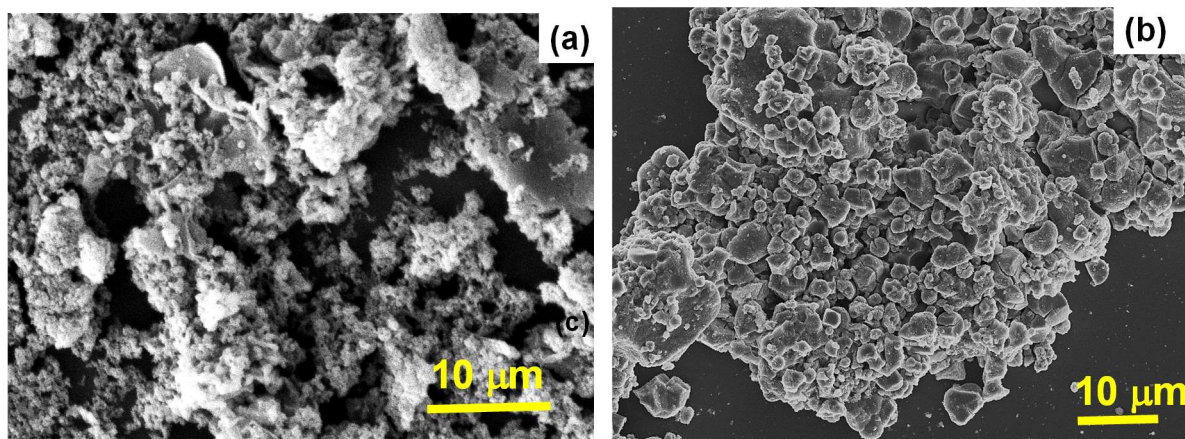


Figure S3. SEM images of bulk PEDOT and bulk PANI obtained from the monomer solution in presence of oxidant without using any surfactant or soft template.

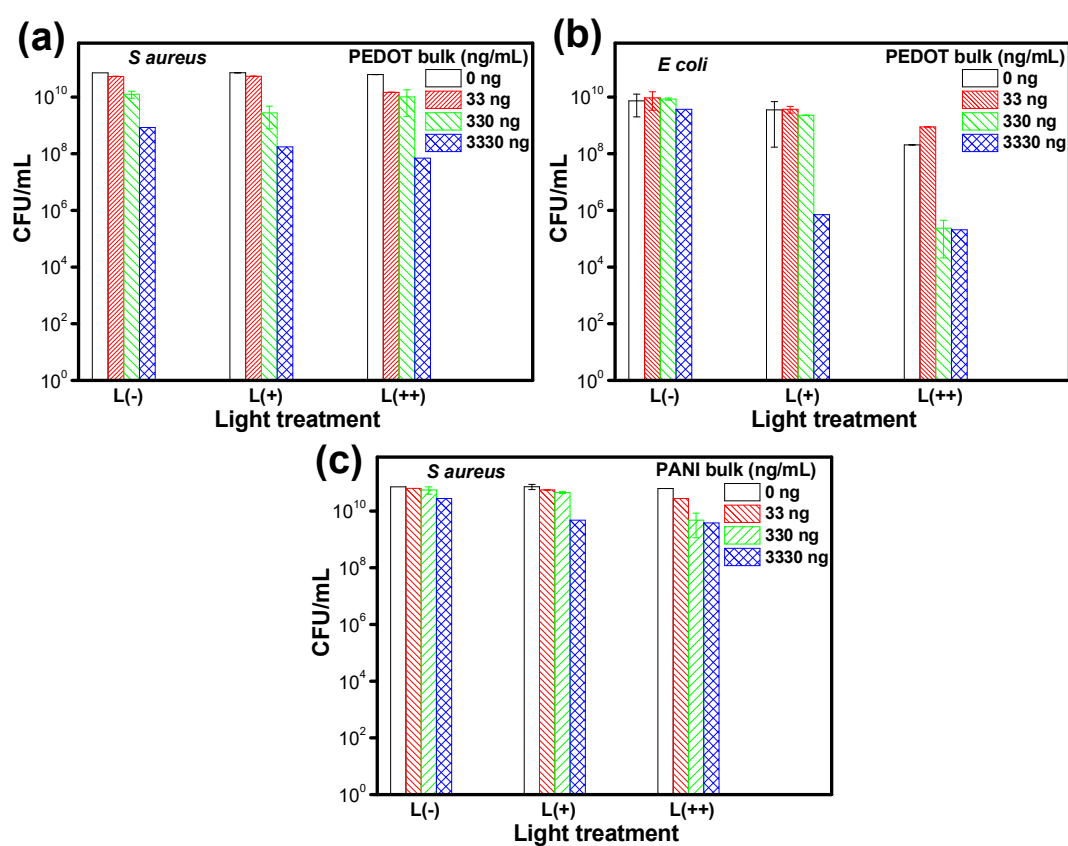


Figure S4. Colony forming units mL⁻¹ of *S. aureus* and *E. coli* cultures in contact with suspensions of (a, b) bulk PEDOT and (c) bulk PANI.